ACS APPLIED NANO MATERIALS

www.acsanm.org Article

A Silver-Chalcogenide Nanomaterial Enveloped with a Carborane-Thiolate Shell for the Electroreduction of CO_2 to CO

Arijit Jana, Zhengyuan Li, Amoghavarsha Ramachandra Kini, Vivek Yadav, Akhil S. Nair, Astrid Campos Mata, Jingjie Wu, Jan Macháček, Tomas Base,* Biswarup Pathak,* Soumyabrata Roy,* and Thalappil Pradeep*

Cite This: https://doi.org/10.1021/acsanm.5c01918 Read Online

ACCESS | Metrics & More | Article Recommendations | Supporting Information

ABSTRACT: Electrocatalytic CO_2 reduction using atomically precise nanomaterials has garnered significant research interest, owing to their controllable molecular structures. Here, we have synthesized an electrocatalyst composed of single crystals having a one-dimensional assembly of silver atoms bridged by sulfur atoms of *meta*-carborane-9-thiolates. The molecular structure of the framework was further characterized through high-resolution ESI-MS, which exhibited silver- and carborane-thiolate-containing ions originating from the fragmentation of the framework. This thermally stable solid acted as an efficient catalyst for the electrocatalytic conversion of CO_2 to CO with a Faradaic efficiency of 85 ± 3%. In situ Raman studies provided experimental verification of binding of CO_2 to the framework. First-principles density functional theory calculations confirmed the feasible adsorption of CO_2 with the Ag chains, highlighting its favorable interaction with the catalyst. Furthermore, free energy calculations revealed the rate-determining step of the conversion process to be the formation of *COOH. This study presents an efficient electrocatalyst featuring a one-dimensional silver-chalcogenide framework.

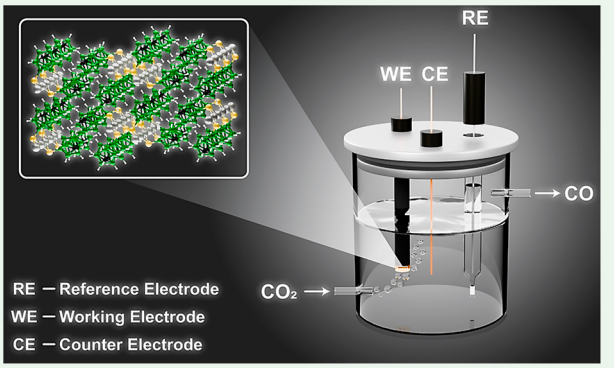

KEYWORDS: *silver-chalcogenide, decarboxylation, solvothermal synthesis, one-dimensional solid, carborane-thiol, CO_2 electroreduction*

INTRODUCTION

The increase in atmospheric CO_2 levels has significantly contributed to global warming, leading to various environmental and societal challenges. Therefore, finding effective methods for CO_2 capture and utilization has become a global priority.[1,2] Techniques such as electrochemical,[3] thermochemical,[4] photochemical,[5] and biochemical catalytic reduction[6] of CO_2 offer promising pathways for converting CO_2 into valuable chemicals and fuels. Among these methods, electrocatalytic CO_2 reduction has gained considerable attention due to its wide range of possible products, the use of water as a key reagent, and its compatibility with renewable electricity sources.[7] Researchers have explored various nano- and microscale materials as catalysts for electrochemical CO_2 reduction, including single-atom catalysts,[8] nanoparticles,[9] nanoclusters,[10] metal−organic frameworks,[11] intermetallic compounds,[12] transition metal dichalcogenides,[13] and perovskites.[14] These materials serve as effective and durable catalysts in the conversion process. Significant efforts have been made to enhance catalyst performance by carefully controlling their size, shape, and composition, which allows for the fine-tuning of their electronic structures.[15−18] Additionally, the choice of solvent and electrolyte type affects catalytic efficiency by influencing CO_2 desolvation and mass transport to the electrodes.[19,20] All these advancements aim to improve overall reaction efficiency and selectivity by designing active catalysts, thereby contributing to the development of effective CO_2 reduction technologies.[21−23]

Atomically precise silver nanomaterials, particularly ligand-protected nanoclusters,[24] nanoparticles,[25] nanowires,[26] nanorings,[27] nanocubes,[28] nanoprisms,[29] and nanocomposites[30] are emerging as active catalysts for electrochemical reduction reactions. Compared to bulk silver metal, nanostructural features like exposed metal atoms, high index facets, and nanoscale pores have enhanced selective CO_2 reduction by promoting active sites that favor specific reactions.[31] In CO_2 electroreduction, a majority of silver-based nanosystems can favor the formation of carbon monoxide (CO) as an end product, thus highlighting the importance of tailoring catalyst design.[32] CO, a key component of syngas, has significant

Received: April 4, 2025
Revised: June 18, 2025
Accepted: June 19, 2025

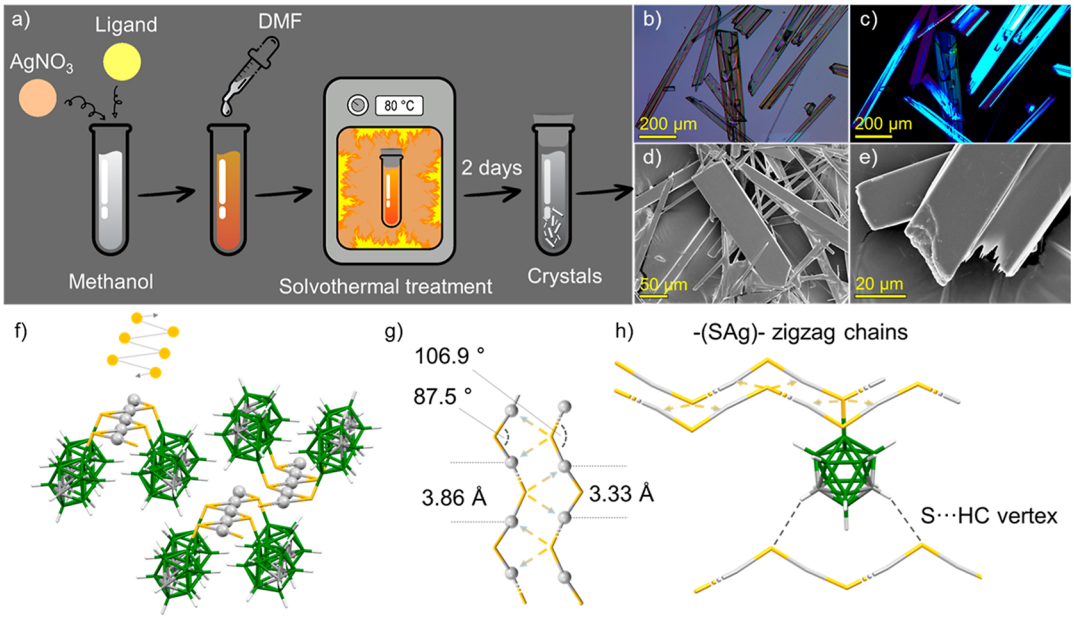

Figure 1. (a) Schematic representation of the synthesis of the Ag-CBT framework in DMF/methanol (3:1, v/v) solvent mixture using a decarboxylation-solvothermal synthesis. Optical micrographs of the as-synthesized microcrystals (b) without polarization and (c) with polarization. FESEM micrographs of the crystals at (d) lower and (e) higher resolution. (f) A small segment of the single-crystal supramolecular framework shows a linear arrangement of Ag atoms within a zigzag-shaped −(SAg)− chain. (g) A top view of two adjacent chains with the depiction of short contact S···Ag interactions pairing them together into a double-chain. (h) Interactions between sulfur atoms of one double-chain and positively charged carborane CH vertices from another, causing two double chains to pack into the 3D framework as depicted in (f). Color code: metallic gray = Ag, yellow = S, green = boron, gray = carbon, and white = hydrogen.

applications in producing synthetic fuels and chemical feedstock via the Fischer−Tropsch process and in the metal processing industry.[19] Specific structural types of silver-based nanocatalysts generate hydrogen gas as a side product along with CO during electrocatalysis of CO_2.[33,34] Therefore, achieving precise structural control is essential to fully harness the potential of nanostructured catalysts for the quantitative production of CO. From this perspective, monolayer-protected silver chalcogenides can offer a new category of precise nanomaterials with tremendous potential as selective CO_2 to the CO electrocatalyst.

Monolayer-protected metal chalcogenides typically consist of a layer of metal atoms or a metal-chalcogenide framework coated with thiol or selenol ligands. These systems can be based on both noble metals, such as gold (Au), silver (Ag), and copper (Cu)[35,36] as well as non-noble metals like lead (Pb), iron (Fe), and tin (Sn).[37,38] Many of these materials exhibit a range of optical activities, characterized by their sharply defined multicolor emissions, in-plane anisotropic electron transport,[39,40] strong exciton stability, and significant electron−phonon coupling.[41,42] A monolayer of surface ligands is crucial for controlling the atomic packing and dimensional growth of these systems. One notable ligand, carborane-thiols, is built from a 12-vertex icosahedral heteroborane cluster, known for its unique geometry, three-dimensional aromaticity, and redox properties.[43−46] This cage-like molecule, along with its metal-containing derivatives, such as complexes,[47,48] clusters,[49−52] and metal−organic frameworks,[53,54] holds significant interest due to its wide-ranging applications in chemistry, biology, and materials science.[55−57] In contrast to these materials, carborane-thiolated silver chalcogenides are rarely mentioned in the literature as active electrocatalysts. As a result, this work focuses on the electroreduction of CO_2 utilizing a carborane-thiolated silver-chalcogenide framework (abbreviated as Ag-CBT).

RESULTS AND DISCUSSION

The Ag-CBT framework was synthesized in 85% yield using a solvothermal process. This process involved mixing silver nitrate ($AgNO_3$) with 1-carboxy-9-thiol-1,7-carborane (referred to as M_9-COOH) in a solvent mixture of dimethylformamide (DMF) and methanol (MeOH) at a volume ratio of 3:1. Figure 1a presents a schematic representation of the synthesis, and the detailed procedure can be found in the Experimental Section. Within 48 h of the solvothermal treatment (at 80 °C), rod-shaped single crystals were formed inside the hydrothermal container. Optical microscopic images of the yellow crystals, exhibiting defined optical polarization, are shown in Figure 1b,c. Scanning electron micrographs (see Figure 1d,e) further confirmed the rod-like shape of the crystals, which had smooth surfaces. Elemental analysis via Energy Dispersive Spectroscopy (EDS) revealed the presence of silver (Ag), sulfur (S), carbon (C), and boron (B) within the crystals (illustrated in Figure S1), consistent with their nominal composition.

Single-crystal X-ray diffraction analysis demonstrated that this framework crystallized in the monoclinic crystal system with the space group $P2_1/m$. The crystallographic refinement and structural parameters of the framework are shown in Tables S1−S4. To investigate the specific role of the M_9-COOH ligand in the synthesis of the Ag-CBT framework, we conducted a reference hydrothermal reaction using 9-thiol-1,7-carborane, referred to as M_9, which is a noncarboxylated derivative of M_9-COOH. This reaction resulted in the formation of hair-like solids, as shown in Figure S2. The powder X-ray diffraction pattern of these solids differed from that of the crystalline Ag-CBT framework, indicating that a

https://doi.org/10.1021/acsanm.5c01918
ACS Appl. Nano Mater. XXXX, XXX, XXX−XXX

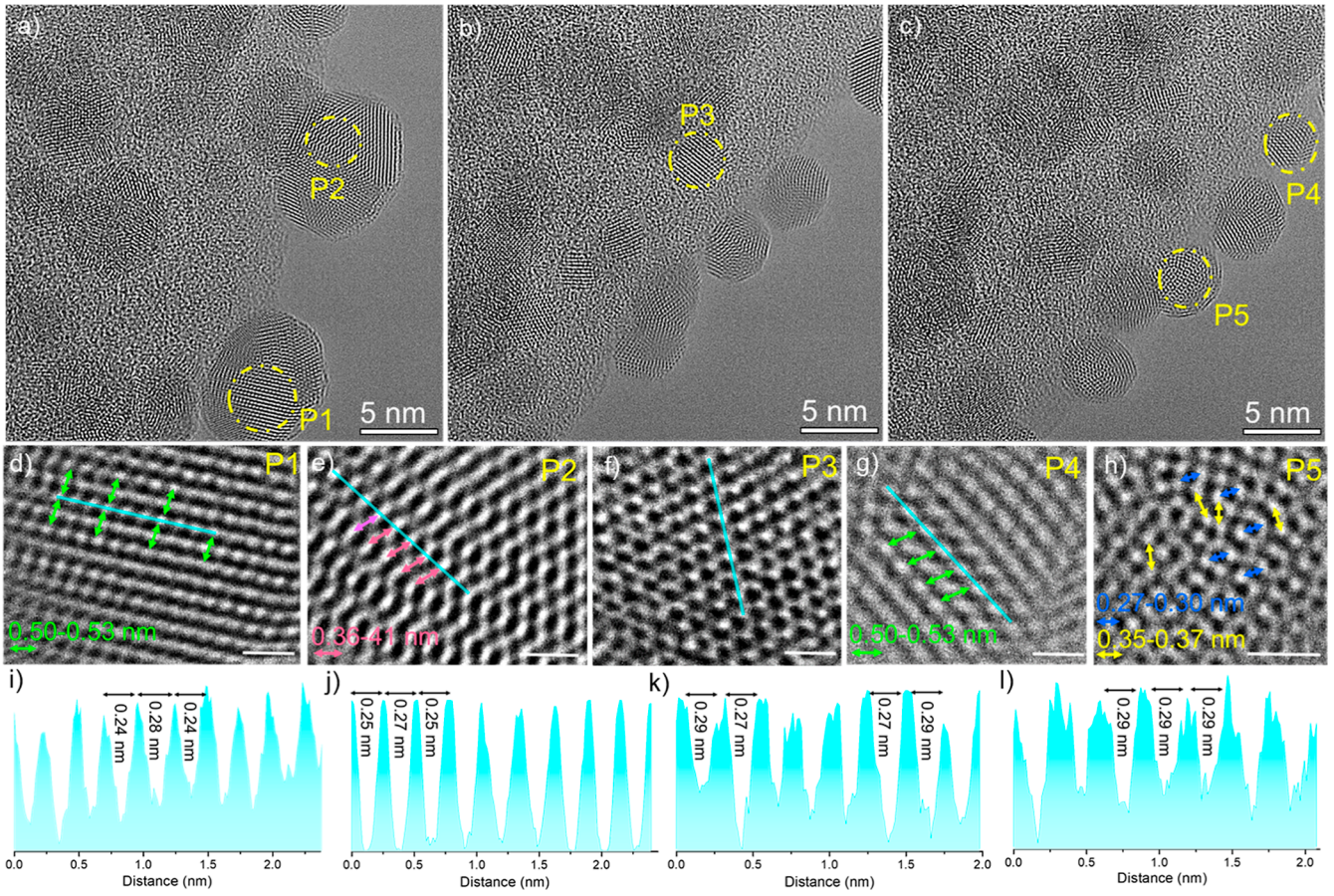

Figure 2. (a–c) Atomic resolution STEM images of three selected regions of the Ag-CBT crystallites. (d–h) Expanded view of the selected regions (marked as P1 to P5) showed linear assembly of Ag atoms in the framework (scale bar, 1 nm). Atomic density distribution in light blue marked lines of (i) P1, (j) P2, (k) P3, and (l) P4 regions.

different compound was formed by using the M_9 ligand (see Figure S3).

The supramolecular organization in single crystals of the Ag-CBT framework showed extended packing, primarily driven by interactions between silver and sulfur atoms (Figure 1f). These atoms formed zigzag −(SAg)− chains, with an interatomic distance of 4.79 Å between adjacent sulfur atoms. This arrangement was similar to the zigzag −(SH) chain reported for the supramolecular packing of the *para*-carborane cluster, which is an analogue of *para*-mercaptobenzoic acid.[58] Notably, in the −(SAg)− chain, half of the sulfur atoms participated in additional short-contact interactions with silver atoms from an adjacent −(SAg)− chain, resulting in the formation of a double-chain structure (Figure 1f,g). Meanwhile, the other half of the sulfur atoms engaged in short-contact interactions with positively charged hydrogen atoms from carborane C−H vertices in another double chain, thus linking the double chains into a three-dimensional supramolecular framework.

In this array, the angles between the Ag−S−Ag units alternated in one chain, measuring 106.9° and 87.53°. The corresponding Ag···Ag distances also alternated, with values of 3.86 and 3.33 Å, while the Ag−S distances were approximately 2.4 Å. The longer Ag···Ag distances suggested a weak argentophilic interaction, similar to what had been observed in other organo-thiolated silver-chalcogenide frameworks.[59−61] A more detailed analysis revealed that the two layers of these indefinite chains interlocked, forming an interesting U-shaped interlocking mechanism, as illustrated in Figure S4. In each interlocked unit, the Ag···Ag distance between the two complementary chains measured 13.50 Å, while the distance to the nearest adjacent Ag chain was 5.35 Å (Figure S5). The primary forces that held these chains together included short intralayer B−H···H−B interactions (ranging from 2.32 to 2.39 Å), as well as interlayer B−H···B (2.97−3.0 Å) and B···B (3.81 Å) van der Waals interactions, all derived from the carborane surroundings (see Figure S6). Additionally, we observed metal-centered interactions: Ag···S (3.16 Å), Ag···H−B (2.83 Å), and Ag···B (3.66 Å) between two neighboring chains also contributed to their extended packing (see Figure S7).

The phase purity of the solids synthesized through hydrothermal methods was confirmed by using powder X-ray diffraction (PXRD). The PXRD patterns displayed exact matching of various reflexes that corresponded to the simulated patterns derived from the single-crystal X-ray diffraction (SCXRD) data (see Figure S8).

Scanning transmission electron microscopy (STEM) investigations revealed a layered arrangement of silver atoms. Low-resolution STEM images indicated the formation of spherical crystallites at the outer periphery of the microcrystals (refer to Figure S9). At higher resolutions, we observed a chain of Ag atoms along the edges of the crystallites (Figure 2a−c). Upon closer examination, we identified a linear arrangement of silver (Ag) atoms in the P1, P2, P3, and P4 regions, as illustrated in Figure 2d−g. Similar arrangements were observed in various other locations. The interatomic distances between these Ag atoms ranged from 0.24 to 0.29 nm, as shown in the atomic

https://doi.org/10.1021/acsanm.5c01918
ACS Appl. Nano Mater. XXXX, XXX, XXX−XXX

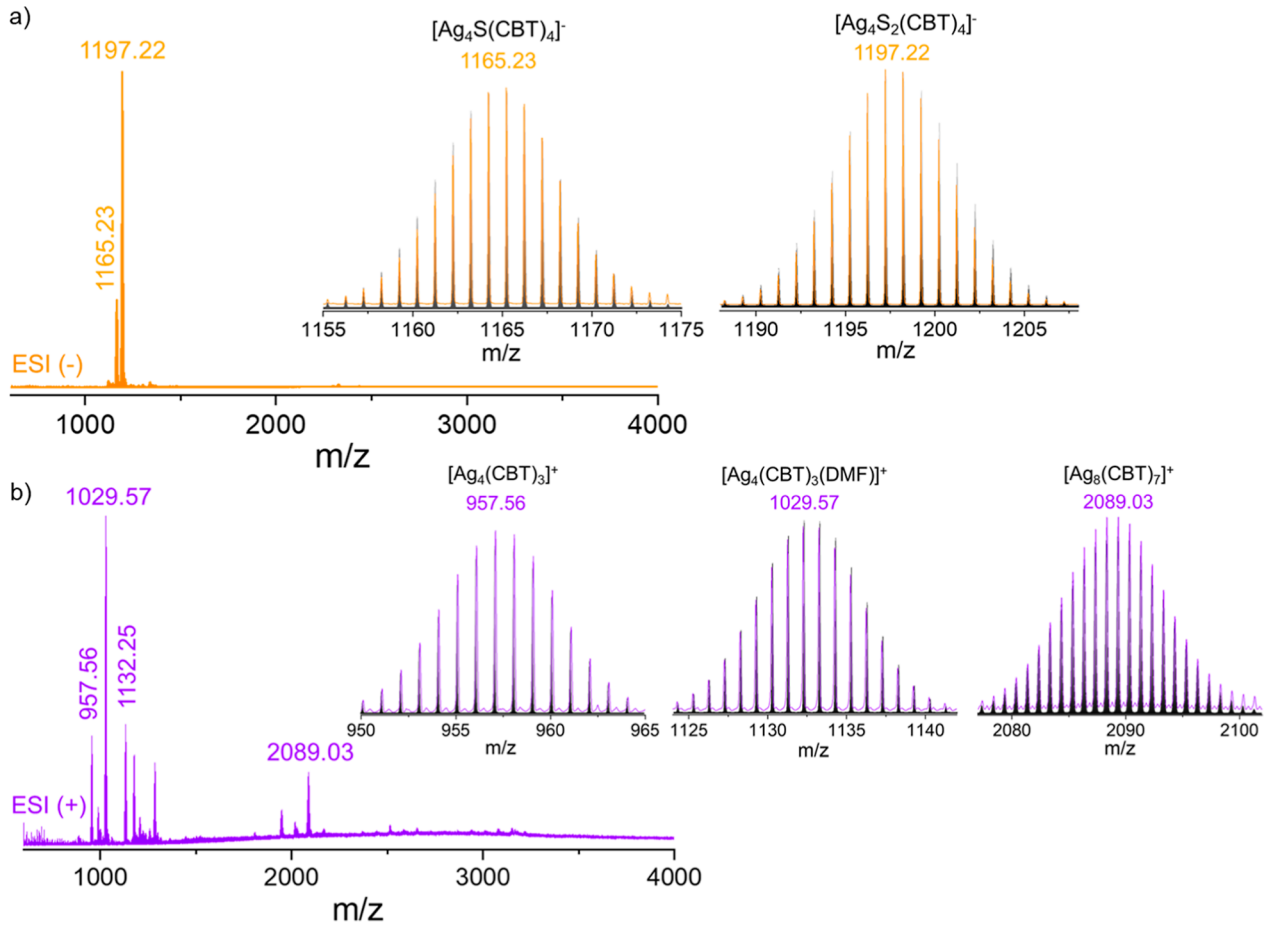

Figure 3. (a) Full range ESI-mass spectrum of the Ag-CBT framework in the negative-ion mode obtained after extraction of the molecular species in DMF. Inset shows the exact matching of the isotopic distribution of the respective fragments. (b) Positive-ion mode ESI-MS spectrum of the Ag-CBT framework. Inset shows the exact matching of the isotopic distribution of the species formed after fragmentation of the framework.

density distribution plots in Figure 2i–l. The slight variation in these distances may be attributed to damage caused by electron beam irradiation and the effects of mechanical exfoliation during sample preparation. Additionally, a random distribution of Ag atoms was also observed in the P5 region (illustrated in Figure 2h), with interatomic distances ranging from 0.27 to 0.30 nm and 0.35 to 0.37 nm. The interatomic distances of 0.35–0.37 nm closely match with the Ag···Ag distances of the framework. Further analysis revealed cross-diagonal distances of 0.50 to 0.53 nm for these Ag layers (P1 and P4 region), which correlated with the interlayer spacing of two nearest adjacent chains, obtained from SCXRD (shown in Figure S5). SCXRD and STEM analyses independently confirmed the unidirectional chain-like assembly of silver atoms within the framework.

The molecular composition of the Ag-CBT framework was analyzed using high-resolution electrospray ionization mass spectrometry (ESI-MS) with a Waters Synapt G2Si mass spectrometer (further details can be found in the Supporting Information). A small portion of the microcrystalline sample was ground in a mortar and then extracted with DMF through centrifugation after 20 min of ultrasonication. In the negative-ion mode ESI-MS, two prominent peaks were observed at m/z = 1165.23 and 1197.22, both with a charge state of 1-. These peaks corresponded to the molecular compositions of $[Ag_4S(CBT)_4]^-$ and $[Ag_4S_2(CBT)_4]^-$, respectively (as shown in Figure 3a).

In contrast, the positive-ion mode ESI-MS (Figure 3b) revealed several peaks with strong intensities, each exhibiting a monocationic charge state at m/z 957.56, 1029.57, and 1132.25. These peaks were identified as $[Ag_4(CBT)_3]^+$, $[Ag_4(CBT)_3(DMF)]^+$, and $[Ag_4(CBT)_4]^+$, respectively. Moreover, a significant peak at m/z 2089.03 (with a charge state of 1+) corresponded to the composition $[Ag_8(CBT)_7]^+$, which resulted from the combination of $[Ag_4(CBT)_3]$ and $[Ag_4(CBT)_4]$ fragments. All of these characteristic peaks correlated well with the one-dimensional framework structure.

The FT-IR and Raman spectroscopic measurements further confirmed the presence of carborane as surface envelopes within the Ag-CBT framework. The FT-IR spectrum of the Ag-CBT framework revealeds vibrational peaks at 3022 and 2599 cm^{-1}, corresponding to the C–H and B–H vibrational bands of the carboranes (see Figure S10). Additionally, we identified vibrational peaks at 1717 cm^{-1} (C═O stretching), 1286 cm^{-1} (C–O stretching), and 2878 cm^{-1} (O–H stretching) in the M_9-COOH ligand, which were absent in the Ag-CBT framework, thereby confirming the decarboxylation of the M_9-COOH ligand. The detection of the icosahedral $-C_2B_{10}H_{11}$ cage breathing vibrational mode at 725 cm^{-1} further supported the presence of carboranes within the Ag-CBT framework. Raman spectroscopic measurements revealed similar observations. The B–H spectral band of the M_9-COOH ligand, which initially exhibited three features at 2611, 2646, and 2672 cm^{-1}, was reduced to a single band centered at

https://doi.org/10.1021/acsanm.5c01918
ACS Appl. Nano Mater. XXXX, XXX, XXX–XXX

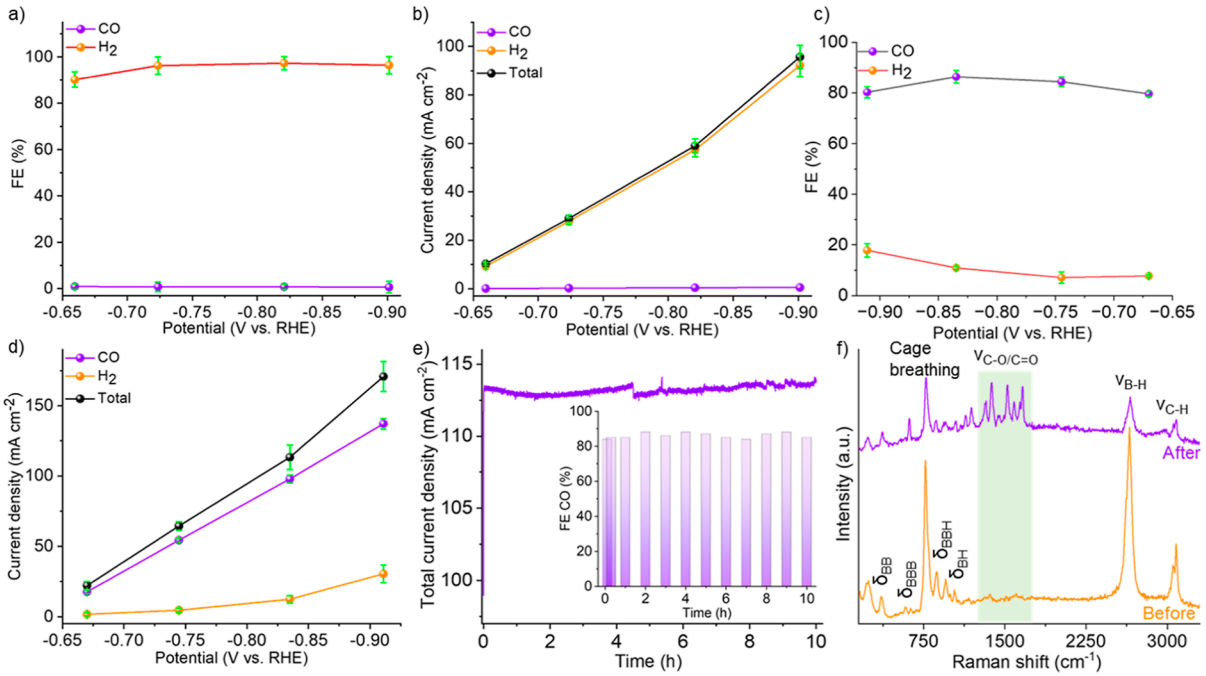

Figure 4. Electrochemical CO_2 reduction reaction using the Ag-CBT framework. (a) Faradaic efficiency and (b) current density of the electrode loaded with the Ag-CBT framework under an argon atmosphere. (c) Faradaic efficiency and (d) current density of the electrode at different potential under a CO_2 atmosphere. (e) Stability of the electrode during the electrocatalytic process. Inset shows time-dependent FE variation of the synthesized CO product using the same electrode. (f) Comparative Raman spectra of the catalyst-loaded electrode before (orange trace) and after (violet trace) CO_2 exposure. Peaks of interest are highlighted here.

2645 cm^{-1} in five different single crystals of the Ag-CBT framework (see Figures S11 and S12). Similarly, the C−H spectral band at 3079 cm^{-1} for the M_9-COOH ligand shifted to 3046 and 3082 cm^{-1} in the Ag-CBT framework. Additionally, three prominent bands at 1290, 1443, and 1682 cm^{-1}, associated with the −COOH group, were absent in the Ag-CBT framework, further indicating that decarboxylation had occurred. To investigate the band gap and associated electronic properties, we measured the solid-state absorption spectrum of the crystalline Ag-CBT sample. The absorption spectrum revealed two distinct bands: a broad, high-energy band ranging from 3.7 to 6.0 eV and a relatively weak, low-energy band between 1.8 and 3.5 eV (see Figure S13). By extrapolating the absorption band edge, we determined the framework's band gaps to be 1.74 and 3.75 eV. The presence of a multiband gap in these materials could facilitate the related electron transfer processes involved in electrocatalytic conversion. Additionally, thermogravimetric analysis (TGA) demonstrated robust thermal stability for the Ag-CBT framework solids, withstanding thermal decomposition initiating at approximately 300 °C (Figure S14). This thermal stability was significantly higher than that of carborane-thiol-protected silver clusters, which exhibited thermal stability between 150 and 200 °C.[62,63]

These framework solids were used as active catalysts to investigate electrocatalytic CO_2 reduction reactions. Initially, we conducted electrocatalysis using a Ag-CBT-loaded gas diffusion electrode in a flow cell. The product analysis revealed that hydrogen (H_2) was the sole product formed in an argon (Ar) atmosphere, achieving a Faradaic efficiency of approximately 90 ± 3% (see Figure 4a,b). Notably, no carbon monoxide (CO) was detected across a wide range of negative potentials (−0.65 to −0.9 V), indicating that CO generation was not possible from the decomposition of the Ag-CBT framework. When supplying CO_2 gas as the feedstock, the Ag-CBT framework maintained stable Faradaic efficiencies for CO production above 80% throughout the entire range of applied potentials studied (see Figure 4c). It may be noted that microcrystalline Ag-CBT framework, characterized by their porous void spaces having 6.5% volume of the unit cell, was suitable for the CO_2 adsorption and subsequent catalytic process (see Figure S15). The maximum Faradaic efficiency for CO reached 86%, with a corresponding partial current density of 98 mA/cm^2 at −0.83 V versus a reversible hydrogen electrode (RHE) (see Figure 4d). The CO partial current density was further increased to 137 mA/cm^2 at −0.91 V vs RHE, while maintaining a Faradaic efficiency of 80% for CO. The Ag-CBT framework was able to retain a steady current density of approximately 113 mA/cm^2 at −0.83 V vs RHE, with consistent CO Faradaic efficiencies of around 86% over a span of 10 h (see Figure 4e). The CO_2 electroreduction measurements conducted at three different pH levels (3, 7.8, and 14) showed that the Faradaic efficiencies for carbon monoxide (CO) were 84.9%, 87.1%, and 86.1% at pH = 3, 7.8, and 14, respectively. In contrast, the Faradaic efficiency for hydrogen was consistently ∼10% across all pH conditions (as shown in Figure S16). These results suggest that the catalyst maintains a robust performance across a wide range of pH levels. A comparison between various silver nanomaterials along with our Ag-CBT framework is shown in Table S5.

A comparative Raman spectroscopic analysis (Figure 4f) revealed that CO_2 was stabilized on the silver-chalcogenide lattice. After CO_2 bubbling, the catalyst-loaded electrode showed five new prominent peaks at 1326, 1371, 1521, 1589, and 1663 cm^{-1}. Note that these features were absent in the parent framework, as mentioned before. While we could not assign the bands to specific binding sites, these vibrational bands corresponded to the symmetric and asymmetric vibrational modes of adsorbed CO_2 and carboxylate anions

https://doi.org/10.1021/acsanm.5c01918
ACS Appl. Nano Mater. XXXX, XXX, XXX−XXX

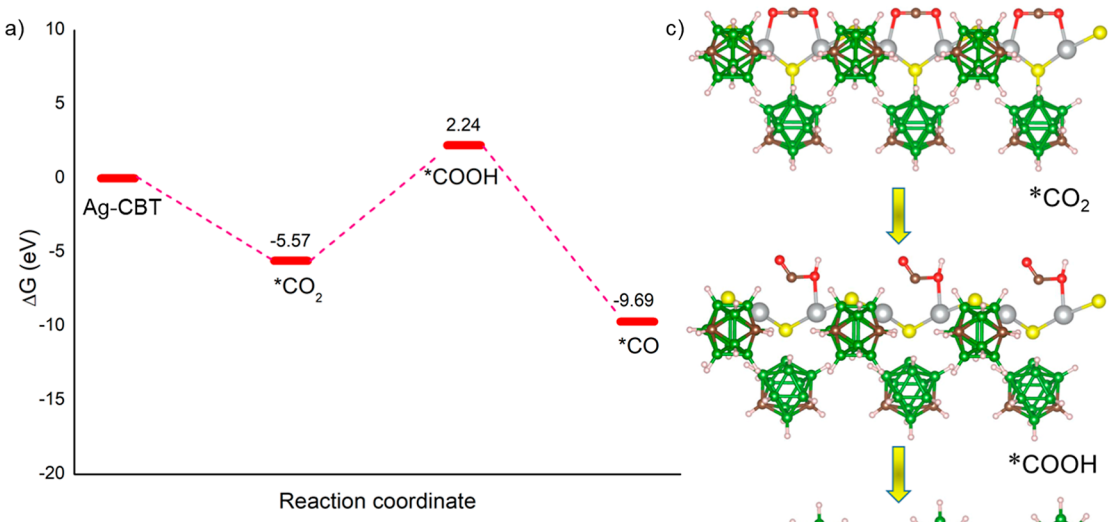

b)

Intermediate	Adsorption energy (eV)
*CO	-7.76
$*CO_2$	-5.57
*COOH	-1.50

Figure 5. DFT calculation of electrochemical CO_2 reduction using the Ag-CBT framework. (a) Free energy diagram of CO_2ER associated with the various intermediate species formed during this conversion. (b) Adsorption efficiencies of different activated species. (c) Schematic representation of the reaction intermediates of CO_2 electroreduction over the one-dimensional framework of the catalyst. Color code: metallic gray: Ag, yellow: S, brown: C, red: O, green: B, and faint pink: H.

on the Ag-CBT framework.[64] Our previous investigation had demonstrated that the binding of adsorbed CO_2 and carboxylate anions significantly influenced the position and intensity of the vibrational bands.[65] Raman spectrum of the M_9-COOH ligand showed the −COOH vibrational bands at 1290, 1443, and 1682 cm^{-1} (Figure S15). Comparative Raman spectra of the Ag-CBT loaded electrode before and after CO_2 exposure with that of pure M_9-COOH suggested that the one-dimensional silver framework is important for CO_2 uptake rather than the carborane cages. Previous studies have also indicated that silver (Ag) centers in various silver complexes, clusters, and nanoparticles can effectively catalyze organic carboxylation reactions by adsorbing CO_2 onto the Ag atoms.[66−68]

Density functional theory (DFT) calculations were conducted to investigate the potential of the Ag-CBT framework as a catalyst for the electrochemical reduction of CO_2. We focused on a reduction pathway involving the formation of COOH, which we identified as the primary rate-determining step in the conversion process. Energetics of the electrochemical reaction were analyzed using the computational hydrogen electrode (CHE) model (see the Supporting Information for details).[69] The reaction energy profile and adsorption configurations of the intermediates are displayed in Figure 5. The results showed that the Ag-CBT framework allows for thermodynamically favorable adsorption of all the involved intermediates: $*CO_2$, *COOH, and *CO. Both *CO and $*CO_2$ exhibited relatively strong adsorption with adsorption energies of −7.76 eV and −5.57 eV, respectively, due to their binding in a bridging configuration. In contrast, *COOH bound to the Ag-CBT framework through a single O atom, resulting in a weaker interaction. This difference in bonding strength made the formation of *COOH the rate-limiting step in the reaction pathway. The subsequent step, involving the dissociation of *COOH to produce *CO, was favored because *CO bound strongly to the Ag-CBT framework. Although the mechanism considered here includes only a limited number of intermediates, the favorable adsorption configurations for the two key intermediates, $*CO_2$ and *CO, suggested that the Ag-CBT framework could serve as a viable catalyst for a broader range of reaction pathways, ultimately leading to the production of other valuable chemicals from the electroreduction of CO_2.

CONCLUSION

In summary, we have developed and characterized a silver-chalcogenide framework featuring a −(SAg)− double chain structure, which is protected by *meta*-carborane-9-thiolate as surface envelopes. This framework was utilized for the electrocatalytic CO_2 reduction. Single-crystal X-ray diffraction (SCXRD) and high-resolution transmission electron microscopy studies confirmed the one-dimensional linear arrangement of silver atoms within the framework. Mass spectrometric analysis revealed that the fragmented species was originating from the framework in the solution. These thermally stable, atomically precise nanomaterials demonstrated efficient CO_2 adsorption and subsequent electroreduction of CO_2 to CO, achieving a Faradaic efficiency of approximately 85% across a wide pH range. Raman spectroscopy highlighted the binding affinity of CO_2 for the 1D silver-chalcogenide framework. Additionally, density functional theory calculations suggested that the Ag···Ag chains enhanced the CO_2 adsorption and facilitated the electroreduction process. This work showcased the synthesis and structural characterization of a robust

https://doi.org/10.1021/acsanm.5c01918
ACS Appl. Nano Mater. XXXX, XXX, XXX−XXX

carborane-thiolate-appended silver-chalcogenide framework with a high capacity for CO_2 electroreduction. It illustrated the potential for diverse electrocatalytic processes using a semiconducting metal-chalcogenide framework, which was stabilized by thermally robust materials and encased in three-dimensional carborane molecular cages.

■ ASSOCIATED CONTENT

Supporting Information

The Supporting Information is available free of charge at https://pubs.acs.org/doi/10.1021/acsanm.5c01918.

Experimental section, instrumentation, computational details, crystallographic information files, and associated spectroscopic and microscopic characterization (PDF)

CIF files for the crystal data of Ag-CBT (CIF)

■ AUTHOR INFORMATION

Corresponding Authors

Tomas Base − *Department of Syntheses, Institute of Inorganic Chemistry, The Czech Academy of Science, Rez 25068, Czech Republic;* orcid.org/0000-0003-2533-8705; Email: tbase@iic.cas.cz

Biswarup Pathak − *Department of Chemistry, Indian Institute of Technology Indore, Indore 453552, India;* orcid.org/0000-0002-9972-9947; Email: biswarup@iiti.ac.in

Soumyabrata Roy − *Department of Materials Science and Nanoengineering, Rice University, Houston, Texas 77005, United States; Department of Sustainable Energy Engineering, Indian Institute of Technology Kanpur, Kanpur, Uttar Pradesh 208016, India*; Email: soumyar@iitk.ac.in

Thalappil Pradeep − *DST Unit of Nanoscience (DST UNS) and Thematic Unit of Excellence (TUE), Department of Chemistry, Indian Institute of Technology Madras, Chennai 600036, India;* orcid.org/0000-0003-3174-534X; Email: pradeep@iitm.ac.in

Authors

Arijit Jana − *DST Unit of Nanoscience (DST UNS) and Thematic Unit of Excellence (TUE), Department of Chemistry, Indian Institute of Technology Madras, Chennai 600036, India*

Zhengyuan Li − *Department of Chemical and Environmental Engineering, University of Cincinnati, Cincinnati, Ohio 45221, United States*

Amoghavarsha Ramachandra Kini − *DST Unit of Nanoscience (DST UNS) and Thematic Unit of Excellence (TUE), Department of Chemistry, Indian Institute of Technology Madras, Chennai 600036, India;* orcid.org/0009-0003-6863-7729

Vivek Yadav − *DST Unit of Nanoscience (DST UNS) and Thematic Unit of Excellence (TUE), Department of Chemistry, Indian Institute of Technology Madras, Chennai 600036, India*

Akhil S. Nair − *Department of Chemistry, Indian Institute of Technology Indore, Indore 453552, India;* orcid.org/0000-0001-5723-3970

Astrid Campos Mata − *Department of Materials Science and Nanoengineering, Rice University, Houston, Texas 77005, United States;* orcid.org/0000-0002-2138-562X

Jingjie Wu − *Department of Chemical and Environmental Engineering, University of Cincinnati, Cincinnati, Ohio 45221, United States*

Jan Macháček − *Department of Syntheses, Institute of Inorganic Chemistry, The Czech Academy of Science, Rez 25068, Czech Republic;* orcid.org/0000-0003-4723-0789

Complete contact information is available at: https://pubs.acs.org/10.1021/acsanm.5c01918

Author Contributions

A.J., A.R.K., and V.Y.: Synthesis, crystallization, and associated characterization of the Ag-CBT framework. Z.L., J.W., and S.R.: Electrocatalytic CO_2 reduction experiments. A.C.M.: STEM measurement. A.S.N. and B.P.: Quantum chemical calculations. J.M. and T.B.: Synthesis and characterization of the carborane derivatives. The first draft of the manuscript is written by A.J. and all authors contributed to finalize the manuscript. T.P. supervised the project and finalized the manuscript.

Notes

The authors declare no competing financial interest.

■ ACKNOWLEDGMENTS

We acknowledge the support of the Science and Engineering Research Board (SERB), Department of Science and Technology (DST), and Government of India. T.P. acknowledges funding from the Centre of Excellence on Molecular Materials and Functions under the Institution of Eminence scheme of IIT Madras. T.P. thanks the Science and Engineering Research Board (SERB), India, for funding through the SPR/2021/000439 research grant. We thank the Sophisticated Analytical Instruments Facility, IIT Madras, and Sudhadevi Antharjanam for the SC-XRD measurements. A.J. thanks IITM for his research fellowship. S.R. acknowledges funding from the Chandrakanta Kesavan Centre for Energy Policy and Climate Solutions, IIT Kanpur (Project No.: DORA/2021136H) and IIT Kanpur research grant IITK/SEE/2024098. A.R.K. thanks the Council of Scientific and Industrial Research (CSIR) for his research fellowship.

■ ABBREVIATIONS

ESI-MS, electrospray ionization mass spectrometry; DFT, density functional theory; EDS, energy dispersive spectroscopy; PXRD, powder X-ray diffraction; SCXRD, single crystal X-ray diffraction; STEM, scanning transmission electron microscopy; TGA, thermogravimetric analysis; CO_2, carbon dioxide; CO, carbon monoxide; ER, electroreduction; CHE, computational hydrogen electrode; DMF, dimethylformamide

■ REFERENCES

(1) Mac Dowell, N.; Fennell, P. S.; Shah, N.; Maitland, G. C. The Role of CO_2 Capture and Utilization in Mitigating Climate Change. *Nat. Clim. Chang.* **2017**, *7* (4), 243−249.

(2) Wei, Y. M.; Kang, J. N.; Liu, L. C.; Li, Q.; Wang, P. T.; Hou, J. J.; Liang, Q. M.; Liao, H.; Huang, S. F.; Yu, B. A Proposed Global Layout of Carbon Capture and Storage in Line with a 2 °C Climate Target. *Nat. Clim. Chang.* **2021**, *11* (2), 112−118.

(3) Nitopi, S.; Bertheussen, E.; Scott, S. B.; Liu, X.; Engstfeld, A. K.; Horch, S.; Seger, B.; Stephens, I. E. L.; Chan, K.; Hahn, C.; Nørskov, J. K.; Jaramillo, T. F.; Chorkendorff, I. Progress and Perspectives of Electrochemical CO_2 Reduction on Copper in Aqueous Electrolyte. *Chem. Rev.* **2019**, *119* (12), 7610−7672.

(4) Roy, S.; Cherevotan, A.; Peter, S. C. Thermochemical CO_2 Hydrogenation to Single Carbon Products: Scientific and Technological Challenges. *ACS Energy Lett.* **2018**, *3* (8), 1938−1966.

(5) Li, X.; Yu, J.; Jaroniec, M.; Chen, X. Cocatalysts for Selective Photoreduction of CO_2 into Solar Fuels. *Chem. Rev.* **2019**, *119* (6), 3962−4179.
(6) Appel, A. M.; Bercaw, J. E.; Bocarsly, A. B.; Dobbek, H.; Dubois, D. L.; Dupuis, M.; Ferry, J. G.; Fujita, E.; Hille, R.; Kenis, P. J. A.; Kerfeld, C. A.; Morris, R. H.; Peden, C. H. F.; Portis, A. R.; Ragsdale, S. W.; Rauchfuss, T. B.; Reek, J. N. H.; Seefeldt, L. C.; Thauer, R. K.; Waldrop, G. L. Frontiers, Opportunities, and Challenges in Biochemical and Chemical Catalysis of CO_2 Fixation. *Chem. Rev.* **2013**, *113* (8), 6621−6658.
(7) Costentin, C.; Robert, M.; Savéant, J. M. Catalysis of the Electrochemical Reduction of Carbon Dioxide. *Chem. Soc. Rev.* **2013**, *42* (6), 2423−2436.
(8) Roy, S.; Li, Z.; Chen, Z.; Mata, A. C.; Kumar, P.; Sarma, S. C.; Teixeira, I. F.; Silva, I. F.; Gao, G.; Tarakina, N. V.; Kibria, M. G.; Singh, C. V.; Wu, J.; Ajayan, P. M. Cooperative Copper Single-Atom Catalyst in 2D Carbon Nitride for Enhanced CO_2 Electrolysis to Methane. *Adv. Mater.* **2024**, *36* (13), 1−13.
(9) Gu, J.; Héroguel, F.; Luterbacher, J.; Hu, X. Densely Packed, Ultra Small SnO Nanoparticles for Enhanced Activity and Selectivity in Electrochemical CO_2 Reduction. *Angew. Chem., Int. Ed.* **2018**, *57* (11), 2943−2947.
(10) Kawawaki, T.; Okada, T.; Hirayama, D.; Negishi, Y. Atomically Precise Metal Nanoclusters as Catalysts for Electrocatalytic CO_2 Reduction. *Green Chem.* **2024**, *26* (1), 122−163.
(11) Song, B.; Liang, Y.; Zhou, Y.; Zhang, L.; Li, H.; Zhu, N. X.; Tang, B. Z.; Zhao, D.; Liu, B. CO_2-Based Stable Porous Metal-Organic Frameworks for CO_2 Utilization. *J. Am. Chem. Soc.* **2024**, *146* (21), 14835−14843.
(12) Wang, J.; Zou, J.; Hu, X.; Ning, S.; Wang, X.; Kang, X.; Chen, S. Heterostructured Intermetallic CuSn Catalysts: High Performance towards the Electrochemical Reduction of CO_2 to Formate. *J. Mater. Chem. A* **2019**, *7* (48), 27514−27521.
(13) Asadi, M.; Kim, K.; Liu, C.; Addepalli, A. V.; Abbasi, P.; Yasaei, P.; Phillips, P.; Behranginia, A.; Cerrato, J. M.; Haasch, R.; Zapol, P.; Kumar, B.; Klie, R. F.; Abiade, J.; Curtiss, L. A.; Salehi-Khojin, A. Nanostructured Transition Metal Dichalcogenide Electrocatalysts for CO_2 Reduction in Ionic Liquid. *Science* **2016**, *353* (6298), 467−470.
(14) Singh, M.; Nama, J.; Paul, T.; Makani, N. H.; Sahoo, A.; Sharma, S.; Banerjee, R. Photoelectrochemically Induced CO_2 Reduction Using Halide-Tunable Lead-Free Perovskites. *ACS Appl. Energy Mater.* **2023**, *6* (6), 3566−3578.
(15) Nabil, S. K.; Roy, S.; Algozeeb, W. A.; Al-Attas, T.; Bari, M. A. a.; Zeraati, A. S.; Kannimuthu, K.; Demingos, P. G.; Rao, A.; Tran, T. N.; Wu, X.; Bollini, P.; Lin, H.; Singh, C. V.; Tour, J. M.; Ajayan, P. M.; Kibria, M. G. Bifunctional Gas Diffusion Electrode Enables In Situ Separation and Conversion of CO_2 to Ethylene from Dilute Stream. *Adv. Mater.* **2023**, *35* (24), 2300389.
(16) Li, Z.; Zhang, T.; Raj, J.; Roy, S.; Wu, J. Revisiting Reaction Kinetics of CO Electroreduction to C_2^+ Products in a Flow Electrolyzer. *Energy Fuels* **2023**, *37* (11), 7904−7910.
(17) Chawla, G.; Sarma, S. C.; Raj, J.; Bagchi, D.; Riyaz, M.; Roy, S.; Mishra, V.; Goud, D.; Peter, S. C. Lattice Charge Tuning-Driven Multi-Carbon Products from Carbon Dioxide. *ACS Sustain. Chem. Eng.* **2024**, *12* (26), 9787−9794.
(18) Dutta, N.; Bagchi, D.; Chawla, G.; Peter, S. C. A Guideline to Determine Faradaic Efficiency in Electrochemical CO_2 Reduction. *ACS Energy Lett.* **2024**, *9* (1), 323−328.
(19) Al-Attas, T.; Nabil, S. K.; Zeraati, A. S.; Shiran, H. S.; Alkayyali, T.; Zargartalebi, M.; Tran, T.; Marei, N. N.; Al Bari, M. A.; Lin, H.; Roy, S.; Ajayan, P. M.; Sinton, D.; Shimizu, G.; Kibria, M. G. Permselective MOF-Based Gas Diffusion Electrode for Direct Conversion of CO_2 from Quasi Flue Gas. *ACS Energy Lett.* **2023**, *8* (1), 107−115.
(20) Marcandalli, G.; Monteiro, M. C. O.; Goyal, A.; Koper, M. T. M. Electrolyte Effects on CO_2 Electrochemical Reduction to CO. *Acc. Chem. Res.* **2022**, *55* (14), 1900−1911.
(21) O'Brien, C. P.; Miao, R. K.; Shayesteh Zeraati, A.; Lee, G.; Sargent, E. H.; Sinton, D. CO_2 Electrolyzers. *Chem. Rev.* **2024**, *124* (7), 3648−3693.
(22) Belsa, B.; Xia, L.; García de Arquer, F. P. CO_2 Electrolysis Technologies: Bridging the Gap toward Scale-up and Commercialization. *ACS Energy Lett.* **2024**, *9* (9), 4293−4305.
(23) Weekes, D. M.; Salvatore, D. A.; Reyes, A.; Huang, A.; Berlinguette, C. P. Electrolytic CO_2 Reduction in a Flow Cell. *Acc. Chem. Res.* **2018**, *51* (4), 910−918.
(24) Seong, H.; Choi, M.; Park, S.; Kim, H. W.; Kim, J.; Kim, W.; Yoo, J. S.; Lee, D. Promoting CO_2-to-CO Electroreduction via the Active-Site Engineering of Atomically Precise Silver Nanoclusters. *ACS Energy Lett.* **2022**, *7* (12), 4177−4184.
(25) Kim, C.; Jeon, H. S.; Eom, T.; Jee, M. S.; Kim, H.; Friend, C. M.; Min, B. K.; Hwang, Y. J. Achieving Selective and Efficient Electrocatalytic Activity for CO_2 Reduction Using Immobilized Silver Nanoparticles. *J. Am. Chem. Soc.* **2015**, *137* (43), 13844−13850.
(26) Liu, S.; Wang, X. Z.; Tao, H.; Li, T.; Liu, Q.; Xu, Z.; Fu, X. Z.; Luo, J. L. Ultrathin 5-Fold Twinned Sub-25 Nm Silver Nanowires Enable Highly Selective Electroreduction of CO_2 to CO. *Nano Energy* **2018**, *45*, 456−462.
(27) Pan, Y.; Paschoalino, W. J.; Bayram, S. S.; Blum, A. S.; Mauzeroll, J. Biosynthesized Silver Nanorings as a Highly Efficient and Selective Electrocatalysts for CO_2 Reduction. *Nanoscale* **2019**, *11* (40), 18595−18603.
(28) Liu, S.; Sun, C.; Xiao, J.; Luo, J. L. Unraveling Structure Sensitivity in CO_2 Electroreduction to Near-Unity CO on Silver Nanocubes. *ACS Catal.* **2020**, *10* (5), 3158−3163.
(29) Qi, K.; Zhang, Y.; Li, J.; Charmette, C.; Ramonda, M.; Cui, X.; Wang, Y.; Zhang, Y.; Wu, H.; Wang, W.; Zhang, X.; Voiry, D. Enhancing the CO_2-to-CO Conversion from 2D Silver Nanoprisms via Superstructure Assembly. *ACS Nano* **2021**, *15* (4), 7682−7693.
(30) Ma, S.; Luo, R.; Gold, J. I.; Yu, A. Z.; Kim, B.; Kenis, P. J. A. Carbon Nanotube Containing Ag Catalyst Layers for Efficient and Selective Reduction of Carbon Dioxide. *J. Mater. Chem. A* **2016**, *4* (22), 8573−8578.
(31) Li, S.; Chen, W.; Dong, X.; Zhu, C.; Chen, A.; Song, Y.; Li, G.; Wei, W.; Sun, Y. Hierarchical Micro/Nanostructured Silver Hollow Fiber Boosts Electroreduction of Carbon Dioxide. *Nat. Commun.* **2022**, *13* (1), 3080.
(32) Kim, C.; Eom, T.; Jee, M. S.; Jung, H.; Kim, H.; Min, B. K.; Hwang, Y. J. Insight into Electrochemical CO_2 Reduction on Surface-Molecule-Mediated Ag Nanoparticles. *ACS Catal.* **2017**, *7* (1), 779−785.
(33) Deng, X.; Alfonso, D.; Nguyen-Phan, T. D.; Kauffman, D. R. Resolving the Size-Dependent Transition between CO_2 Reduction Reaction and H_2 Evolution Reaction Selectivity in Sub-5 Nm Silver Nanoparticle Electrocatalysts. *ACS Catal.* **2022**, *12* (10), 5921−5929.
(34) Deng, X.; Alfonso, D.; Nguyen-Phan, T. D.; Kauffman, D. R. Breaking the Limit of Size-Dependent CO_2RR Selectivity in Silver Nanoparticle Electrocatalysts through Electronic Metal-Carbon Interactions. *ACS Catal.* **2023**, *13* (23), 15301−15309.
(35) Yan, H.; Hohman, J. N.; Li, F. H.; Jia, C.; Solis-Ibarra, D.; Wu, B.; Dahl, J. E. P.; Carlson, R. M. K.; Tkachenko, B. A.; Fokin, A. A.; Schreiner, P. R.; Vailionis, A.; Kim, T. R.; Devereaux, T. P.; Shen, Z. X.; Melosh, N. A. Hybrid Metal-Organic Chalcogenide Nanowires with Electrically Conductive Inorganic Core through Diamondoid-Directed Assembly. *Nat. Mater.* **2017**, *16* (3), 349−355.
(36) Sun, P.; Xie, M.; Zhang, L.-M.; Liu, J.-X.; Wu, J.; Li, D.-S.; Yuan, S.-F.; Wu, T.; Li, D. Ultrastable Anti-Acid Shield in Layered Silver Coordination Polymers. *Angew. Chem., Int. Ed.* **2022**, *61* (44), No. e202209971.
(37) Yang, H.; Mandal, S.; Lee, Y. H.; Park, J. Y.; Zhao, H.; Yuan, C.; Huang, L.; Chen, M.; Dou, L. Dimensionality Engineering of Lead Organic Chalcogenide Semiconductors. *J. Am. Chem. Soc.* **2023**, *145* (44), 23963−23971.
(38) Krebs, B.; Henkel, G. Transition-Metal Thiolates: From Molecular Fragments of Sulfidic Solids to Models for Active Centers in Biomolecules. *Angew. Chem., Int. Ed.* **1991**, *30*, 769−788.

https://doi.org/10.1021/acsanm.5c01918
ACS Appl. Nano Mater. XXXX, XXX, XXX−XXX

(39) Paritmongkol, W.; Lee, W. S.; Shcherbakov-Wu, W.; Ha, S. K.; Sakurada, T.; Oh, S. J.; Tisdale, W. A. Morphological Control of 2D Hybrid Organic-Inorganic Semiconductor AgSePh. *ACS Nano* **2022**, *16* (2), 2054−2065.
(40) Paritmongkol, W.; Sakurada, T.; Lee, W. S.; Wan, R.; Müller, P.; Tisdale, W. A. Size and Quality Enhancement of 2D Semiconducting Metal-Organic Chalcogenolates by Amine Addition. *J. Am. Chem. Soc.* **2021**, *143* (48), 20256−20263.
(41) Lee, W. S.; Cho, Y.; Powers, E. R.; Paritmongkol, W.; Sakurada, T.; Kulik, H. J.; Tisdale, W. A. Light Emission in 2D Silver Phenylchalcogenolates. *ACS Nano* **2022**, *16* (12), 20318−20328.
(42) Hernandez Oendra, A. C.; Aspect, M. A.; Jaeggi, J. L.; Baumann, J.; Lightner, C. R.; Pun, A. B.; Norris, D. J. Tunable Synthesis of Metal-Organic Chalcogenide Semiconductor Nanocrystals. *Chem. Mater.* **2023**, *35* (21), 9390−9398.
(43) Mingos, M. P. In *50th Anniversary of Electron Counting Paradigms for Polyhedral Molecules*; Mingos, M. P., Ed.; Springer, 2021.
(44) Poater, J.; Escayola, S.; Poater, A.; Teixidor, F.; Ottosson, H.; Viñas, C.; Solà, M. Single-Not Double-3D-Aromaticity in an Oxidized Closo Icosahedral Dodecaiodo-Dodecaborate Cluster. *J. Am. Chem. Soc.* **2023**, *145* (41), 22527−22538.
(45) Fisher, S. P.; Tomich, A. W.; Lovera, S. O.; Kleinsasser, J. F.; Guo, J.; Asay, M. J.; Nelson, H. M.; Lavallo, V. Nonclassical Applications of Closo-Carborane Anions: From Main Group Chemistry and Catalysis to Energy Storage. *Chem. Rev.* **2019**, *119* (14), 8262−8290.
(46) Núñez, R.; Tarre's, M.; Ferrer-Ugalde, A.; De Biani, F. F.; Teixidor, F. Electrochemistry and Photoluminescence of Icosahedral Carboranes, Boranes, Metallacarboranes, and Their Derivatives. *Chem. Rev.* **2016**, *116* (23), 14307−14378.
(47) Kirlikovali, K. O.; Axtell, J. C.; Gonzalez, A.; Phung, A. C.; Khan, S. I.; Spokoyny, A. M. Luminescent Metal Complexes Featuring Photophysically Innocent Boron Cluster Ligands. *Chem. Sci.* **2016**, *7* (8), 5132−5138.
(48) Hablot, D.; Ziessel, R.; Alamiry, M. A. H.; Bahraidah, E.; Harriman, A. Nanomechanical Properties of Molecular-Scale Bridges as Visualised by Intramolecular Electronic Energy Transfer. *Chem. Sci.* **2013**, *4* (1), 444−453.
(49) Yadav, V.; Jana, A.; Acharya, S.; Malola, S.; Nagar, H.; Sharma, A.; Kini, A. R.; Antharjanam, S.; Machacek, J.; Adarsh, K. N. V. D.; Base, T.; Häkkinen, H.; Pradeep, T. Site-Specific Substitution in Atomically Precise Carboranethiol-Protected Nanoclusters and Concomitant Changes in Electronic Properties. *Nat. Commun.* **2025**, *16* (1), 1197.
(50) Jana, A.; Jash, M.; Dar, W. A.; Roy, J.; Chakraborty, P.; Paramasivam, G.; Lebedkin, S.; Kirakci, K.; Manna, S.; Antharjanam, S.; Machacek, J.; Kucerakova, M.; Ghosh, S.; Lang, K.; Kappes, M. M.; Base, T.; Pradeep, T. Carborane-Thiol Protected Copper Nanoclusters: Stimuli-Responsive Materials with Tunable Phosphorescence. *Chem. Sci.* **2023**, *14* (6), 1613−1626.
(51) Kini, A. R.; Debta, S.; Jana, A.; Aparna, C.; Yadav, V.; Kusiak, N.; Base, T.; Waghmare, U. V.; Ghosh, P.; Pradeep, T. Nanomechanical Investigations of Crystals of Copper Nanocluster Isomorphs: Enhanced Hardness of the Low-Density Analogue. *Chem. Mater.* **2025**, *37*, 1284−1296.
(52) Jana, A.; Spoorthi, B. K.; Nair, A. S.; Nagar, A.; Pathak, B.; Base, T.; Pradeep, T. A. Luminescent Cu_4 Cluster Film Grown by Electrospray Deposition: A Nitroaromatic Vapour Sensor. *Nanoscale* **2023**, *15* (18), 8141−8147.
(53) Huang, J. H.; Si, Y.; Dong, X. Y.; Wang, Z. Y.; Liu, L. Y.; Zang, S. Q.; Mak, T. C. W. Symmetry Breaking of Atomically Precise Fullerene-like Metal Nanoclusters. *J. Am. Chem. Soc.* **2021**, *143* (32), 12439−12444.
(54) Jana, A.; Duary, S.; Das, A.; Kini, A. R.; Acharya, S.; Machacek, J.; Pathak, B.; Base, T.; Pradeep, T. Multicolor Photoluminescence of Cu_{14} Clusters Modulated Using Surface Ligands. *Chem. Sci.* **2024**, *15* (34), 13741−13752.
(55) Kennedy, R. D.; Krungleviciute, V.; Clingerman, D. J.; Mondloch, J. E.; Peng, Y.; Wilmer, C. E.; Sarjeant, A. A.; Snurr, R. Q.; Hupp, J. T.; Yildirim, T.; Farha, O. K.; Mirkin, C. A. Carborane-Based Metal-Organic Framework with High Methane and Hydrogen Storage Capacities. *Chem. Mater.* **2013**, *25* (17), 3539−3543.
(56) Bae, Y. S.; Farha, O. K.; Spokoyny, A. M.; Mirkin, C. A.; Hupp, J. T.; Snurr, R. Q. Carborane-Based Metal-Organic Frameworks as Highly Selective Sorbents for CO_2 over Methane. *Chem. Commun.* **2008**, *0* (35), 4135−4137.
(57) Idrees, K. B.; Kirlikovali, K. O.; Setter, C.; Xie, H.; Brand, H.; Lal, B.; Sha, F.; Smoljan, C. S.; Wang, X.; Islamoglu, T.; Macreadie, L. K.; Farha, O. K. Robust Carborane-Based Metal-Organic Frameworks for Hexane Separation. *J. Am. Chem. Soc.* **2023**, *145* (43), 23433−23441.
(58) Thomas, J. C.; Boldog, I.; Auluck, H. S.; Bereciartua, P. J.; Dušek, M.; Macháček, J.; Bastl, Z.; Weiss, P. S.; Baše, T. Self-Assembled p-Carborane Analogue of p-Mercaptobenzoic Acid on Au{111. *Chem. Mater.* **2015**, *27* (15), 5425−5435.
(59) Veselska, O.; Demessence, A. d^{10} Coinage Metal Organic Chalcogenolates: From Oligomers to Coordination Polymers. *Coord. Chem. Rev.* **2018**, *355*, 240−270.
(60) Wang, G.-E.; Luo, S.; Di, T.; Fu, Z.; Xu, G. Layered Organic Metal Chalcogenides (OMCs): From Bulk to Two-Dimensional Materials. *Angew. Chem., Int. Ed.* **2022**, *61* (27), No. e202203151.
(61) Schriber, E. A.; Paley, D. W.; Bolotovsky, R.; Rosenberg, D. J.; Sierra, R. G.; Aquila, A.; Mendez, D.; Poitevin, F.; Blaschke, J. P.; Bhowmick, A.; Kelly, R. P.; Hunter, M.; Hayes, B.; Popple, D. C.; Yeung, M.; Pareja-Rivera, C.; Lisova, S.; Tono, K.; Sugahara, M.; Owada, S.; Kuykendall, T.; Yao, K.; Schuck, P. J.; Solis-Ibarra, D.; Sauter, N. K.; Brewster, A. S.; Hohman, J. N. Chemical Crystallography by Serial Femtosecond X-Ray Diffraction. *Nature* **2022**, *601* (7893), 360−365.
(62) Jana, A.; Jash, M.; Poonia, A. K.; Paramasivam, G.; Islam, M. R.; Chakraborty, P.; Antharjanam, S.; Machacek, J.; Ghosh, S.; Adarsh, K. N. V. D.; Base, T.; Pradeep, T. Light-Activated Intercluster Conversion of an Atomically Precise Silver Nanocluster. *ACS Nano* **2021**, *15* (10), 15781−15793.
(63) Jana, A.; Unnikrishnan, P. M.; Poonia, A. K.; Roy, J.; Jash, M.; Paramasivam, G.; Machacek, J.; Adarsh, K. N. V. D.; Base, T.; Pradeep, T. Carboranethiol-Protected Propeller-Shaped Photoresponsive Silver Nanomolecule. *Inorg. Chem.* **2022**, *61* (23), 8593−8603.
(64) Hadjiivanov, K. I.; Panayotov, D. A.; Mihaylov, M. Y.; Ivanova, E. Z.; Chakarova, K. K.; Andonova, S. M.; Drenchev, N. L. Power of Infrared and Raman Spectroscopies to Characterize Metal-Organic Frameworks and Investigate Their Interaction with Guest Molecules. *Chem. Rev.* **2021**, *121* (3), 1286−1424.
(65) Ahuja, T.; Chaudhari, K.; Paramasivam, G.; Ragupathy, G.; Mohanty, J. S.; Pradeep, T. Toward Vibrational Tomography of Citrate on Dynamically Changing Individual Silver Nanoparticles. *J. Phys. Chem. C* **2021**, *125* (6), 3553−3566.
(66) Sekine, K.; Yamada, T. Silver-Catalyzed Carboxylation. *Chem. Soc. Rev.* **2016**, *45* (16), 4524−4532.
(67) Liu, Y.; Chai, X.; Cai, X.; Chen, M.; Jin, R.; Ding, W.; Zhu, Y. Central Doping of a Foreign Atom into the Silver Cluster for Catalytic Conversion of CO_2 toward C−C Bond Formation. *Angew. Chem., Int. Ed.* **2018**, *57* (31), 9775−9779.
(68) Yu, D.; Tan, M. X.; Zhang, Y. Carboxylation of Terminal Alkynes with Carbon Dioxide Catalyzed by Poly (N-Heterocyclic Carbene)-Supported Silver Nanoparticles. *Adv. Synth. Catal.* **2012**, *354*, 969−974.
(69) Nørskov, J. K.; Rossmeisl, J.; Logadottir, A.; Lindqvist, L.; Kitchin, J. R.; Bligaard, T.; Jónsson, H. Origin of the Overpotential for Oxygen Reduction at a Fuel-Cell Cathode. *J. Phys. Chem. B* **2004**, *108* (46), 17886−17892.

https://doi.org/10.1021/acsanm.5c01918
ACS Appl. Nano Mater. XXXX, XXX, XXX−XXX